

Steam reforming of methane over a nickel-based catalyst

Rakhi ^{a,*}, Vivien Günther ^b, Jana Richter ^a, Fabian Mauss ^a

^a Brandenburg University of Technology, 03046 Cottbus, Germany,

^b LOGE AB, 03044 Cottbus, Germany

* rakhi.rakhi@b-tu.de

Abstract

Steam reforming is a promising route to convert natural gas into syngas - a mixture of H₂ and CO, used as a feed stock e.g. for ammonia, methanol and Fischer-Tropsch synthesis processes. For the industrial application of steam reforming, a detailed understanding of the process is a prerequisite. Models that capture the detailed homogeneous and heterogeneous reaction kinetics and the comprehensive transport processes as well as their interaction have the potential to optimize the catalytic process without expensive experimental campaigns. In the present work, a one-dimensional model, LOGEcat is used to carry out a detailed investigation considering a multi-step reaction mechanism for modeling steam reforming of methane over nickel-based catalyst. The model is computationally cost effective due to the reduction in dimensionality, in contrast to experimental investigations which are not always feasible or 2D/3D simulations which are computationally expensive. The 1D tool is based on a series of perfectly stirred reactors (PSR) and is applicable to the simulation of all standard after-treatment catalytic processes of combustion exhaust gas as well as other chemical processes involving heterogeneous catalysis such as the Sabatier process. We have applied the model to perform the simulations for various reactor conditions in terms of parameters such as temperature, pressure, velocity and steam-to-carbon (S/C) ratio. Several chemical reaction terms have been analyzed and the results are compared with 2D simulation and experimental reference data. We note a very good agreement of the various profiles produced with the cost-effective reduced order model in comparison to the reference data.

Keywords: Nickel-based catalyst; One-dimensional modeling; Methane; Steam reforming;

1. Introduction

Steam reforming of hydrocarbons is a crucial chemical process [1, 2] providing synthesis gas (H₂ and CO) which plays a key role as a feedstock in many catalytic processes, for example, synthesis of methanol, oxo-synthesis, and Fischer-Tropsch synthesis [3]. The produced synthesis gas, hydrogen, is used in the manufacturing of ammonia [3]. The most prominent and widely used industrial steam reforming process is the methane or gas (natural) reforming. This is one of the most efficient technologies for hydrogen and synthesis gas production from fossil fuels in large scale facilities reaching yields close to the thermodynamic equilibrium [2, 3]. Thus, conventional steam reformers deliver high concentrations of hydrogen at high fuel conversion rates [4], however, this process is disadvantageous in small scale operation units because of the highly endothermic reactions and the requirement of efficient external energy supply.

Thermodynamics control the products of the reaction and favour the formation of methane at lower temperature along with hydrogen at higher ones. Steam reforming of methane accompanied by water-gas shift reactions on a Ni/MgAl₂O₄ catalyst by intrinsic rate equations derived from a Langmuir-Hinshelwood mechanism is described in [5]. Recently, a catalytic sequence for reactions of CH₄ with CO₂ and H₂O on Ni/MgO catalysts has been postulated in [6] and a microkinetic model for steam reforming reactions over a Ni/MgAl₂O₄ catalyst has been proposed in [7] by reactions for CO₂ reforming of

methane and deactivation by carbon formation.

Due to the potential to reduce the cost of synthesis gas production and environmental concerns, partial oxidation over noble metal catalysts [8–11] as well as CO₂ reforming [12–14] of natural gas to synthesis gas have attained much interest. The sequence and interaction of the reaction routes have been considered in several investigations in order to understand the reaction mechanism of synthesis gas formation from methane. Earlier, a direct catalytic partial oxidation route has been followed [11], however, in later studies the overall conversion is realized in a two-step process (indirect route) [8–10, 15]. In [11, 15–17], steps for steam reforming for the catalytic partial oxidation of methane over platinum and rhodium are published. The reaction kinetics of methane steam reforming over nickel catalyst has been extensively investigated experimentally and theoretically in [18, 19].

All the investigations discussed above are either performed experimentally (not always feasible) or using 2D/3D tools which are computationally expensive specially when the full reaction mechanism is included. The computational cost increases drastically with increasing number of species and alternatives need to be explored in order to capture the flow physics and chemistry at a reduced cost. A good strategy is to reduce the reaction mechanism or dimensionality from 2D/3D to 1D which are time efficient alternatives and are suitably applicable to catalyst simulations.

In this paper, selecting the latter approach (reduction in dimensions) a one-dimensional model which is discussed in next section, has been elaborated to test the steam reforming of methane over nickel/alumina monoliths in the temperature interval of 900-1350 K. The results are compared with the data available in the literature, for the 2D simulations as well as experiments. Note that this work forms the basis for further detailed investigations presented in our recent study [20].

2. Model Description

The one-dimensional model, LOGecat [21] is used for the simulations presented in this paper. The model is based on the single-channel 1D catalyst model and is applicable to the simulation of all standard after-treatment catalytic processes of combustion exhaust gas, for example, three-way catalyst (TWC), diesel oxidation catalysts (DOC), NO_x storage and reduction (NSR) catalysts and selective catalytic reduction (SCR) catalysts.

The model has been successfully applied and tested in previous studies [20, 22]. However, a detailed investigation of the steam reforming of methane over nickel has not been done in any of the previous studies. So, here we aim to analyze the case considered in a general and detailed way in order to check the predictability of model and to know how far the one-dimensional model can capture the flow physics and the chemistry involved with it.

Now, we discuss the modeling of the conservation and flow equations for the readability of this paper. A number of representative channels are used to model the three-way catalytic converter. The gas and surface properties are calculated as a function of axial distance in these channels and also, the heat conduction between the channels is modeled. In contrast, no radial heat conduction between the channels is considered in case of a single-channel (discussed below) set-up representing the whole catalyst using one channel.

2.1. Single Channel Model

Figure 1 shows the single channel which is divided into a finite number of cells with Δx as their length. Each cell is treated as a perfectly stirred reactor (PSR) and the pressure gradient along with inhomogeneity of the mixture can be neglected as the diameter of the catalytic channel is small. A thin layer represented by a separate pore gas zone close to the wall is used to model the external diffusion and this pore layer is depicted by the area between the bulk gas and the washcoat as shown in the figure.

The model used to carry out the simulations is the part of the LOGEsoft software suite [21] for chemical reaction calculation. The conservation equations (next section) for gas species mass fraction, gas enthalpy, surface temperature, pore layer gas species mass fraction, and surface site fractions are solved in each PSR. These equations are solved for each time step and additionally, the 1D Navier-Stokes equations for pressure as well as flow velocity are solved over all cells by an operator splitting method.

2.1.1. Conservation Equations

Assuming constant pressure during the time step Δt in the operator splitting loop, the bulk gas in each cell is modeled by a PSR. The mass transfer coefficient accounts for the species transport between bulk gas and pore volume layer and the conservation equation for bulk gas species mass fraction is given as,

$$\begin{aligned} \rho \frac{\partial Y_{i,g}}{\partial t} = & \frac{(\rho v)_{in} A}{V_g} (Y_{i,in} - Y_{i,g}) + W_i \omega_{i,g} \\ & - \frac{P \Delta x}{V_g} W_i K_m k_{m,i} (C_{i,g} - C_{i,p}) \\ & + Y_{i,g} \frac{P \Delta x}{V_g} \sum_{j=1}^{N_g} W_j K_m k_{m,j} (C_{j,g} - C_{j,p}) \end{aligned} \quad (1)$$

The subscript g denotes the bulk gas, in the inflow from the upstream cell and p gas in the pore layer. $Y_{i,g}$ is the mass fraction of species i , V_g is the gas volume in the current cell, $w_{i,g}$ is the species source term for gas phase reaction, K_m is the tunable parameter for the overall mass transfer, $k_{m,i}$ is the conservation mass transfer coefficient of species i , $C_{i,g}$ is the concentration of species i in the bulk gas, and $C_{i,p}$ is the concentration of species i in the pore layer and P is the geometric wetted perimeter of the channel. For more details we refer the reader to [21].

The pore volume layer considers gas phase as well as surface reactions which further includes diffusion into the pores and the conservation equation of the gas phase species is given as,

$$\begin{aligned} \rho_{p,l} \frac{\partial Y_{i,p,l}}{\partial t} = & \frac{P \Delta x}{V_{p,l}} W_i K_m k_{m,i} (C_{i,g} \\ & - C_{i,p,l})|_{l=1} + W_i \omega_{i,p,l} \\ & + W_i K_e \sum_{m=1}^{N_{surf}} \frac{A_m}{V_{p,l}} \omega_{i,m} \\ & + D_i \frac{C_{i,p,l} - C_{i,p,l+1}}{W_{l+1,l}} \frac{A_m}{V_{p,l}} \\ & - Y_{i,p,l} \sum_{j=1}^{N_g} \left[\frac{P \Delta x}{V_{p,l}} K_m k_{m,j} W_j (C_{j,g} \right. \\ & \left. - C_{j,p,l})|_{l=1} + W_j K_e \sum_{m=1}^{N_{surf}} \frac{A_m}{V_{p,l}} \omega_{j,m} \right. \\ & \left. + D_i \frac{C_{j,p,l} - C_{j,p,l+1}}{W_{l+1,l}} \frac{A_m}{V_{p,l}} \right] \end{aligned} \quad (2)$$

In the above equation, $V_{p,l}$ is the gas volume of the pore volume layer in washcoat layer l in the current cell, $w_{i,p,l}$ is the species source term for gas phase reactions in the pore layer in washcoat layer l , N_{surf} is the number of different surface materials present in the catalytic converter (usually 1), A_m is the catalytic surface area in the current cell, k_e is the tuning parameter for the overall reaction efficiency. The parameter D_i accounts for an additional term for diffusion through multiple washcoat layers and is appropriate diffusion coefficient for species i , the subscript l is the current washcoat layer, $w_{l+1,l}$ is the radial distance through the washcoat calculated as $(w_{l+1} - w_l)/2$ for diffusion between washcoat layer l and $l + 1$. Note that the source term for bulk gas species transport into the washcoat is only used for the first washcoat layer (denoted as $|_{l=1}$).

Next, the conservation equation for surface species site fraction is given as,

$$\frac{\partial \theta_{i,n}}{\partial t} = \sigma_{i,n} K_e \frac{\omega_{i,n}}{\tau_n} \quad (3)$$

$\Theta_{i,n}$ indicates the site fraction of species i at site n , τ_n is the site density, $w_{i,n}$ is the species source term from

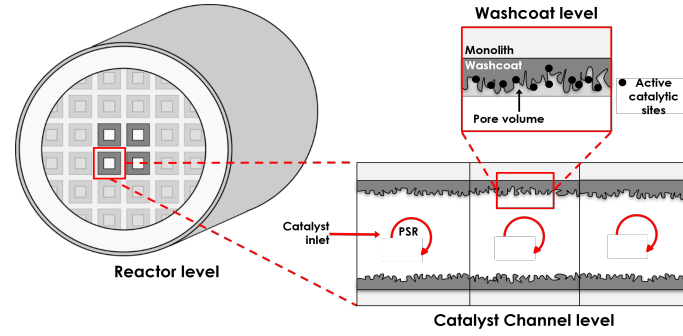


Figure 1: Schematic illustration of the modeling approach

reactions at site n and $\sigma_{i,n}$ is the site occupancy number of species i at site n .

The heat transport by convection and molecular transport is taken into account by the bulk energy (specific enthalpy) conservation equation given as,

$$\begin{aligned} \frac{\partial h_g}{\partial t} = & -K_h h_T \frac{P \Delta x}{m_g} (T_g - T_w) + \frac{(\rho v)_{in} A}{m_g} (h_{in} - h_g) \\ & + \frac{P \Delta x}{m_g} \sum_{j=1}^{N_g} W_j K_m k_{m,j} (C_{j,g} \\ & - C_{j,p}) (h_g - h_{j,g \leftrightarrow p}) \end{aligned} \quad (4)$$

In equation 4, h_g is the bulk gas specific enthalpy, h_T is the convective heat transfer coefficient between bulk gas and surface, T_g is the bulk gas temperature, T_w the pore layer temperature, h_{in} is the specific enthalpy of the gas from the upstream cell and $h_{j,g \rightarrow p}$ the specific enthalpy of species j transported between the bulk gas and the pore layer. The bulk gas enthalpy is used in case of the species being transported from the bulk gas and pore layer enthalpy is used if it is transported to the bulk gas.

The pore layer temperature is assumed to be homogeneous for the substrate as well as for the gas and the pressure is assumed constant in the pore layer. The kinetic energy due to gas movement is neglected. Considering these assumptions, the conservation equation for the surface temperature is given as,

$$\begin{aligned} & (\rho_s V_s c_{p,s} + \rho_p V_p c_{p,p}) \frac{\partial T_w}{\partial t} \\ = & \\ & V_s \frac{\partial}{\partial x} \left(k_s \frac{\partial T_w}{\partial x} \right) + K_h h_T P \Delta x (T_g - T_w) \\ & - \sum_{j=1}^{N_{g,p}} W_j P \Delta x K_m k_{m,j} (C_{j,g} \\ & - C_{j,p}) (h_{j,p} - h_{j,g \leftrightarrow p}) \\ & - \sum_{j=1}^{N_{g,p}} W_j \left[h_{j,p} V_p K_e \omega_{j,p} + h_{j,p} K_e \sum_{m=1}^{N_m} A_m \omega_{j,m} \right] \\ & - K_e \sum_{m=1}^{N_m} \sum_{j=1}^{N_{s,m}} h_{j,m} W_j A_m \omega_{j,m} \\ & + \frac{k_{s,l+1} \left(\frac{\partial T_{w,l+1}}{\partial w_{l+1,l-1}} \right) - k_{s,l-1} \left(\frac{\partial T_{w,l-1}}{\partial w_{l+1,l-1}} \right)}{w_l} \end{aligned} \quad (5)$$

where, V_s is the volume of the solid wall material (washcoat and substrate) in the current cell, $C_{p,s}$ is the specific heat capacity of the solid material at constant pressure, $C_{p,p}$ is the specific heat capacity in the pore volume layer at constant pressure and K_h is a tunable parameter for the heat transfer. Hence, the above equation accounts for heat conduction along the channel, heat convection/ diffusion to the bulk gas, molecular heat transport as well as heat released by reactions. $k_{s,l}$ is the thermal conductivity of washcoat layer l and for single washcoat pore diffusion is mimicked by the tunable parameter k_e . The washcoat diffusion for the surface temperature is also included in case if there are multiple washcoats. Additionally, heat flow term is used to account for heat losses through the material and the catalyst at the periphery of the substrate.

The heat and mass transfer coefficients, h_T and $k_{m,i}$, used in the conservation equations are calculated from the Nusselt and Sherwood numbers [23]. For simultaneously developing velocity, concentration and thermal boundary layer flow, the correlations for Sherwood and Nusselt numbers are used as [24],

$$Sh_i(x) = \begin{cases} \frac{0.35}{Sc_i^{1/6}} \sqrt{\left(\frac{d_h}{4}\right)^2 v}, & 0 < x < \frac{\left(\frac{d_h}{4}\right)^2 v}{D_i} \left(\frac{1}{Sc_i}\right)^{1/3} \left(\frac{1.4}{Sh_{T,\infty}}\right)^2 \\ Sh_{T,\infty}, & x \geq \frac{\left(\frac{d_h}{4}\right)^2 v}{D_i} \left(\frac{1}{Sc_i}\right)^{1/3} \left(\frac{1.4}{Sh_{T,\infty}}\right)^2 \end{cases} \quad (6)$$

$$Nu(x) = \begin{cases} \frac{0.35}{Pr^{1/6}} \sqrt{\left(\frac{d_h}{4}\right)^2 v}, & 0 < x < \frac{\left(\frac{d_h}{4}\right)^2 v}{D_T} \left(\frac{1}{Pr}\right)^{1/3} \left(\frac{1.4}{Nu_{T,\infty}}\right)^2 \\ Nu_{T,\infty}, & x \geq \frac{\left(\frac{d_h}{4}\right)^2 v}{D_T} \left(\frac{1}{Pr}\right)^{1/3} \left(\frac{1.4}{Nu_{T,\infty}}\right)^2 \end{cases} \quad (7)$$

Here, D_i is the species diffusion coefficient for species i , D_T is the thermal diffusion coefficient, v is the fluid velocity along the channel and $Sh_{T,\infty}$ and $Nu_{T,\infty}$ are the asymptotic Sherwood and Nusselt numbers, respectively, for constant flux boundary conditions (their values are taken from [25]). The Schmidt number for species i , Sc_i and the Prandtl number, Pr are given as,

$$Sc_i = \frac{\mu_i}{\rho D_i} \quad (8)$$

$$Pr = \frac{c_p \mu}{k_g} \quad (9)$$

where, μ_i is the dynamic viscosity, D_i is the diffusion coefficient of species i , C_p is the heat capacity at constant pressure, μ is the dynamic viscosity and k_g is the thermal conductivity of the gas.

2.1.2. Flow equations

With the assumption that the flow is in steady state, the conservation equations are given as,

$$\frac{\partial(\rho v)}{\partial x} = -\frac{A_{w,G}}{m_g} \sum_{i=1}^{N_g} W_i k_{m,i} (C_{i,g} - C_{i,p}) \quad (10)$$

$$\frac{\partial(\rho v^2)}{\partial x} + \frac{\partial p}{\partial x} = -\frac{f_F}{2} (\rho v) \left| v \right| \frac{p}{A} \quad (11)$$

as mass and momentum equations, respectively. In the above equations, A is the cross-sectional channel area. The friction factor, f_F for laminar and fully developed flow is given as,

$$f_F = \frac{16}{Re} = \frac{16\mu}{\rho v d_h} \quad (12)$$

For more details related to the model and the derivations for the equations, we refer the reader to [21].

3. Surface reaction mechanism

We have used the reaction mechanism from [3] which contains 6 gas-phase and 13 surface species in total. The reaction mechanism consists of 42 reactions. The reaction mechanism indicates that adsorbed carbon species (CH, CH₂, CH₃ etc) formed from activated methane reacts with adsorbed atomic oxygen O(s), formed from the adsorption of oxygen or from the decomposition of water and CO₂, and produce carbon oxide. The mechanism also comprises the reactions of partial oxidation and steam reforming of methane and is based on the key reaction intermediate - adsorbed atomic oxygen O(s). For the details of the reaction mechanism, we refer the reader to [3].

Note that the sticking coefficients are used as kinetic data for the adsorption of reactants and products (H₂, O₂, CH₄, H₂O, CO, CO₂) given in the reaction mechanism.

3.1. Thermodynamic Consistency

The equilibrium of a chemical reaction is given as,

$$\sum_i v'_{ik} A_i \rightleftharpoons \sum_i v''_{ik} A_i \quad (13)$$

and is defined by the thermodynamic properties of the participating species. In terms of equilibrium constant, K_{pk} , the equilibrium activities, a_i , obey the expression,

$$K_{pk} = \prod_i (a_i^{eq})^{v_{ik}} = \exp\left(-\frac{\Delta_k G^0}{RT}\right) \quad (14)$$

$v_{ik} = v_{ik}^l - v_{ik}^r$ is the stoichiometric coefficient, R gas constant and T temperature. The change of free enthalpy at normal pressure p^0 is given as,

$$\Delta_k G^0 = \sum_i v_{ik} G_i^0(T) \quad (15)$$

The activation can be approximated by their partial pressure in case of gases and by coverage in case of surface species. Considering the dependence of the heat capacity on temperature by a forth-order polynomial and standard

enthalpies and entropies of formation, in that case the standard free enthalpies can be expressed in terms of seven coefficients,

$$G_i^0(T) = a_{0,i} + a_{1,i}T + a_{2,i}T^2 + a_{3,i}T^3 + a_{4,i}T^4 + a_{5,i}T^5 + a_{6,i}T \ln T \quad (16)$$

The rate coefficients for the forward and the reverse reaction must obey the below equation to predict the equilibrium correctly,

$$\frac{k_{fk}}{k_{rk}} = K_{pk} \prod_i (c_i^0)^{v_{ik}} \quad (17)$$

where, c_i are reference concentrations at normal pressure. Nonetheless, the forward and the reverse reactions are defined separately with their own rate laws due to the problems encountered in setting up a reaction mechanism. It is difficult to define the thermodynamic data for intermediate surface species. The thermodynamic consistency is ensured in a sense that the thermodynamic equilibrium of the participating gas-phase species is matched for a range of temperatures, while writing all reversible reactions as pairs of independent forward and backward reactions. The thermodynamic data of the intermediate species is, therefore not needed for the evaluation of the reaction rates [3]. We do not aim to cover the more details in this section and hence leave this to the readers interest. Note that the reaction mechanism and the thermodynamic data for all the species used in the present study are taken from [26].

4. Simulation Set-up

The simulation set-up used for the present study follows from [3]. The investigation is extended for different reactor conditions in terms of parameters, such as, temperature, S/C ratio, flow rate and pressure. Analysis is done for four different temperatures, T=920, 1020, 1120, and 1220 K while keeping all other parameters (S/C, \dot{f} and P) constant. Similarly, the S/C ratio is varied as S/C=1.9, 2.77, and 3.67, flow rate as \dot{f} =296, 593 and 1186 mL/min and pressure as P=1, 10 and 100 atm with other parameters fixed.

We have considered a single channel being 3.0×10^{-2} m in length with a catalyst radius of 7.5×10^{-3} m (640 cpsi) and it is uniformly divided into 25 cells. One layer of washcoat is used for the simulations. The overall heat transfer efficiency factor, mass transfer efficiency factor and efficiency factors for surface chemistry are taken as unity. The surface site density, τ for Ni is 2.6×10^{-5} mol/m² [2]. The surface area per catalyst length is used as 6.9×10^{-2} m²/m. 75% Argon dilution is used.

5. Results

The model explained above is used to perform the simulations of steam reforming of methane over a nickel catalyst and all the kinetic parameters are taken from [3]. Some of the important terms encountered in chemical reaction engineering are conversion, selectivity and yield which are discussed in the following section. It is important to check these quantities to observe if the system is consistent. The variation of these quantities are shown with different temperature. The conversion describes the ratio of how much of a reactant has reacted and lies between zero and one. The yield shows the formation of a desired product and it also falls in between zero and one. The selectivity defines the ratio of the desired product to

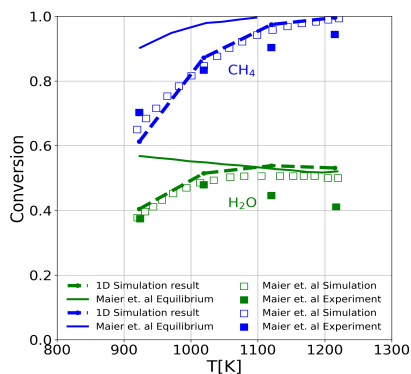


Figure 2: Methane and water conversion as a function of temperature for $S/C=2.77$ and 75% Ar along with the reference data.

the undesired products. The formulas for these quantities are given where they are first discussed in the section.

Figure 2 shows the conversion of methane and water as a function of temperature along with the reference data. The conversion is calculated as, $X_i = (y_{i,o} - y_{i,e})/y_{i,o}$. The simulations are performed for fixed S/C ratio as 2.77 and 75% Argon dilution. The 1D simulation results using LOGEcat model are in very good agreement with the experimental and simulation results from [3]. It is observed that the thermodynamic equilibrium is attained at the higher temperatures. However, at higher temperature the simulation results, both from LOGEcat model as well as 2D reference data, deviates from the experimental data.

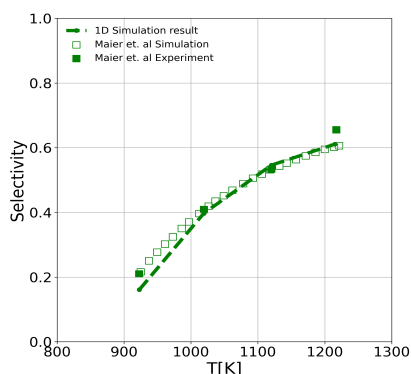


Figure 3: CO Selectivity variation with temperature in methane steam reforming for $S/C=2.77$ and 75% Ar along with the reference data.

The CO selectivity variation with temperature in methane steam reforming for fixed S/C ratio is shown in Figure 3 along with the reference simulation and experimental data. The selectivity for CO is calculated as, $S_{CO} = X_{CO}/(X_{CO} + X_{CO_2} + X_{CH_4})$ and we observe a very good agreement for the 1D LOGEcat model results with [3].

Figure 4 illustrates the H_2/CO ratio variation with the temperature in methane steam reforming for S/C ratio 2.77 and 75% Argon along with the reference results. As explained in [3], the over-prediction of the H_2/CO ratio in comparison to the experimental measurements at the given S/C ratio might be due to the underestimation of water-gas shift reaction at low temperature in the 2D as well as 1D model. The H_2/CO ratio for simulation, Maier's 2D simulation as well as results from 1D model, is higher

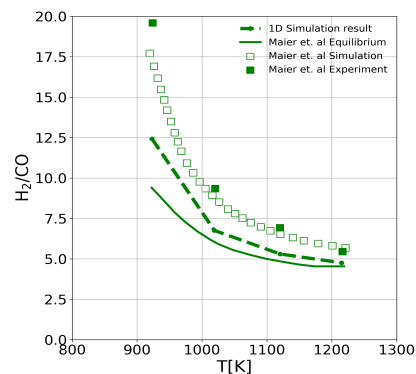


Figure 4: H_2/CO ratio variation with temperature in methane steam reforming for $S/C=2.77$ and 75% Ar along with the reference data.

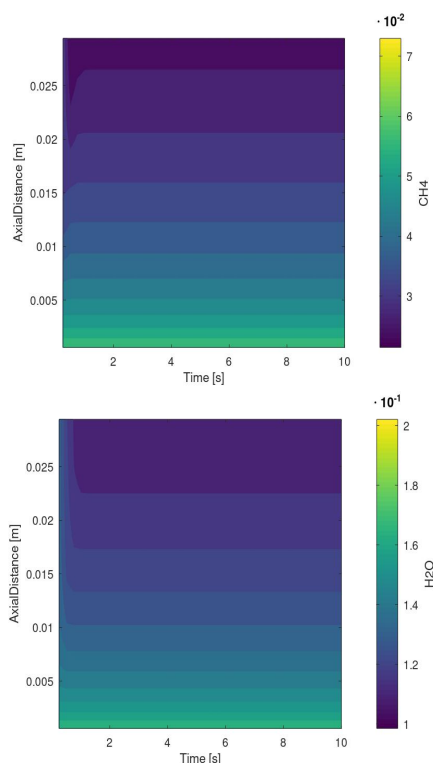


Figure 5: (a) Methane and (b) water concentration along the reactor for $T=920$ K.

compared to the equilibrium calculation at temperature ≤ 1000 K. The 1D results lie in between the experimental and simulation results from [3]. Nevertheless, it is worth noticing that the 1D model capture this profile, qualitatively as well as quantitatively very well.

Further, the variation of concentration for reactants and products along with the axial distance/ length of the reactor is shown in Figure 5 and 6. The simulation results are shown for $T=920$ K. These figures show that the reactants (Figure 5), methane and water, are being used in the first few seconds, i.e., within 2s. Then the thermal equilibrium is reached and no change in the concentration can be observed after 2s but the simulations do run a little longer in order to make sure that steady state is reached. Similarly, the formation of products (Figure 6), H_2 , CO , CO_2 , takes place within first few seconds and then it

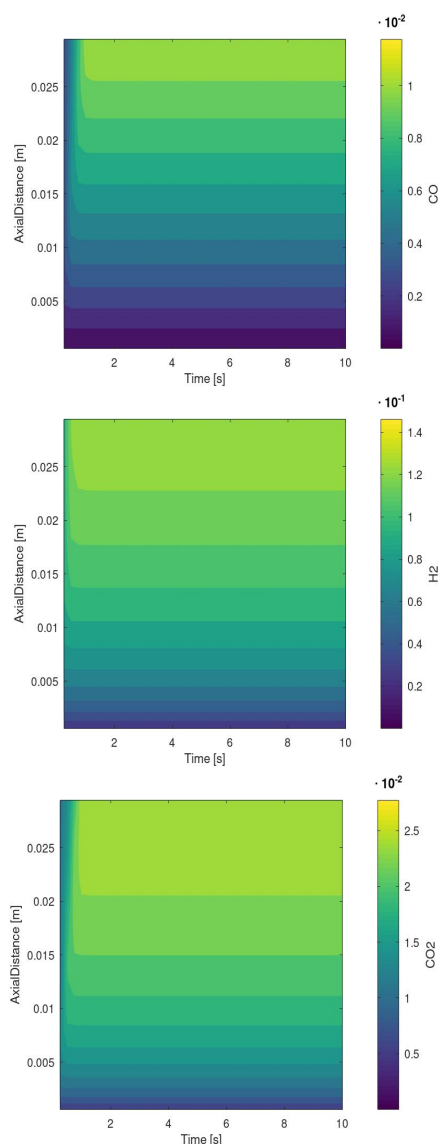


Figure 6: (a) CO, (b) H₂ and (c) CO₂ concentration along the reactor for T=920 K.

ceases. We expect this behaviour as the endothermic reactions are dominant on the catalytic surface in the initial phase which cause the major changes in concentration of different species only in the beginning and then the system attains thermal equilibrium. However, if we observe these concentration plots at higher temperature (not shown in this paper due to limited space), it takes slightly longer to reach steady state and hence, it depends on the temperature.

In Figure 7, the methane and water conversion is shown as a function of temperature for fixed S/C ratio (S/C=3) along with the reference data. The figure captures the conversion behaviour for a wide range of temperature, T \in [600, 1300] in order to check the predictability of the 1D model for higher temperature. The 1D simulation results are in good agreement with the reference 2D simulations and experiments for the entire temperature range. The reference data is available only for methane conversion, however, we have also shown the water conversion for the given temperature range for our simulation set-up.

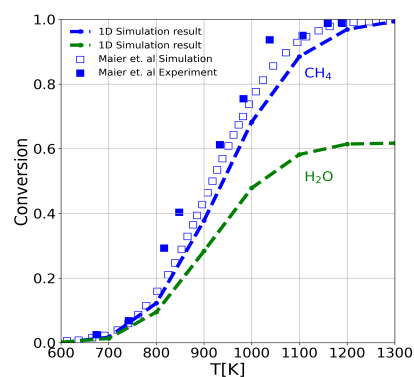


Figure 7: Methane and water conversion as a function of temperature for S/C=3 along with the reference data.

6. Conclusions

This paper presents the kinetics of the steam reforming of methane over nickel catalyst using a one-dimensional tool, LOGEcat. The results are compared with literature [3] and the investigation is carried out for different temperatures. Various quantities, such as, selectivity, yield and conversion has been discussed.

The results show that the conversion, selectivity, H₂/CO ratio for temperature \in [920, 1020, 1120, 1220] K are in very good agreement with the reference data considered for the comparison purpose. This proves the capability of the model to capture the basic flow physics and the chemistry and hence, the model can be used in multiple directions for further investigations at a reduced computational cost.

Acknowledgment

The authors thank the Graduate Research School (GRS) of the BTU Cottbus-Senftenberg for the financial support.

References

- [1] B. T. Schädel, M. Duisberg, and O. Deutschmann, "Steam reforming of methane, ethane, propane, butane, and natural gas over a rhodium-based catalyst," *Catalysis Today*, vol. 142, pp. 42–51, 2009.
- [2] J. R. Rostrup-Nielsen, In: *Anderson JR, Boudart M (eds) Catalytic steam reforming in catalysis—science and technology*. Berlin: Springer-Verlag, 1984.
- [3] L. Maier, B. Schädel, K. H. Delgado, S. Tischer, and O. Deutschmann, "Steam Reforming of Methane Over Nickel: Development of a Multi-Step Surface Reaction Mechanism," *Topics in Catalysis*, vol. 54, pp. 845–858, 2011.
- [4] B. C. Michael, A. Donazzi, and L. D. Schmidt, "Effects of H₂O and CO₂ addition in catalytic partial oxidation of methane on Rh," *Journal of Catalysis*, vol. 265, pp. 117–129, 2009.
- [5] R. Quiceno, O. Deutschmann, J. Warnatz, and J. Pérez-Ramírez, "Modelling of the high-temperature catalytic partial oxidation of methane over platinum gauze. Detailed gas-phase and surface chemistries coupled with 3D flow field simulations," *Applied Catalysis A*, vol. 303, pp. 166–176, 2006.
- [6] J. Wei and E. Iglesia, "Isotopic and kinetic assessment of the mechanism of reactions of CH₄ with CO₂ or H₂O to form synthesis gas and carbon on nickel catalysts," *Journal of Catalysis*, vol. 224, pp. 370–383, 2004.
- [7] L. M. Aparicio, "Transient Isotopic Studies and Microkinetic Modeling of Methane Reforming over Nickel Catalysts," *Journal of Catalysis*, vol. 165, pp. 262–274, 1997.
- [8] D. Dissanayake, M. P. Rosynek, K. C. C. Kharas, and J. H. Lunsford, "Partial Oxidation of Methane to Carbon

- Monoxide and Hydrogen over a Ni/Al₂O₃ Catalyst,” *Catalysis Today.*, vol. 132, pp. 117–127, 1991.
- [9] W. J. M. Vermeiren, E. Blomsma, and P. A. Jacobs, “Catalytic and thermodynamic approach of the oxyreforming reaction of methane,” *Catalysis Today.*, vol. 13, pp. 427–436, 1992.
- [10] S. Hannemann, J. D. Grunwaldt, N. van Vegten, A. Baiker, P. Boye, and C. G. Schroer, “Distinct Spatial Changes of the Catalyst Structure inside a Fixed-Bed Microreactor during the Partial Oxidation of Methane over Rh/Al₂O₃,” *Catalysis Today.*, vol. 126, p. 54, 2007.
- [11] D. A. Hickman and L. D. Schmidt, “Steps in CH₄ oxidation on Pt and Rh surfaces: High-temperature reactor simulations,” *American Institute of Chemical Engineers AIChE.*, vol. 39, pp. 1164–1177, 1993.
- [12] A. M. Gadalla and M. E. Sommer, “Carbon dioxide reforming of methane on nickel catalysts,” *Chemical Engineering Science.*, vol. 44, pp. 2825–2829, 1989.
- [13] Z. W. Liu, H. S. Roh, and K. W. Jun, “Important factors on carbon dioxide reforming of methane over nickel-based catalysts,” *Journal of Industrial and Engineering Chemistry.*, vol. 9, pp. 753–761, 2003.
- [14] M. C. J. Bradford and M. A. Vannice, “Catalytic reforming of methane with carbon dioxide over nickel catalysts II. Reaction kinetics,” *Applied Catalysis A: General.*, vol. 142, pp. 97–122, 1996.
- [15] R. Schwiedernoch, S. Tischer, C. Correa, and O. Deutschmann, “Experimental and Numerical Study of the Transient Behavior of a Catalytic Partial Oxidation Monolith,” *Chemical Engineering Science.*, vol. 58(3), pp. 633–642, 2003.
- [16] O. Deutschmann and L. Schmidt, “Modeling the partial oxidation of methane in a short-contact-time reactor,” *American Institute of Chemical Engineers AIChE.*, vol. 44, pp. 2465–2477, 1998.
- [17] A. B. Mhadeshwar and D. G. J. Vlachos, “Hierarchical Multiscale Mechanism Development for Methane Partial Oxidation and Reforming and for Thermal Decomposition of Oxygenates on Rh,” *The Journal of Physical Chemistry: B.*, vol. 109(35), pp. 16819–16835, 2005.
- [18] J. Xu and G. F. Froment, “Methane steam reforming, methanation and water-gas shift: I. Intrinsic kinetics,” *American Institute of Chemical Engineers AIChE.*, vol. 35, pp. 88–96, 1989.
- [19] J. R. Rostrup-Nielsen and J. H. B. Hansen, “CO₂-Reforming of Methane over Transition Metals,” *Journal of Catalysis.*, vol. 144, pp. 38–49, 1993.
- [20] Rakhi., V. Günther, J. Richter, and F. Mauss, “Steam reforming of methane over nickel catalyst using a one-dimensional model,” *International Journal of Environmental Science.*, vol. 5(1), pp. 1–32, 2022.
- [21] “LOGEsoft v1.10.” www.logesoft.com, 2008.
- [22] K. Fröjd and F. Mauss, “A Three-Parameter Transient 1D Catalyst Model,” *SAE International Journal of Engines.*, vol. 4 (1), pp. 1747–1763, 2011.
- [23] F. Incopera, D. DeWitt, T. Bergman, and S. Lavine, “Fundamentals of Heat and Mass Transfer 6E,” 2006.
- [24] K. Ramanathan, V. Balakotaiah, and D. West, “Light-off criterion and transient analysis of catalytic monoliths,” *Chemical Engineering Science.*, vol. 58, pp. 1381–1405, 2003.
- [25] H. Santos and M. Costa, “Modelling transport phenomena and chemical reactions in automotive three-way catalytic converters,” *Chemical Engineering Journal.*, vol. 148, pp. 173–183, 2009.
- [26] D. Schmider, L. Maier, and O. Deutschmann, “Reaction Kinetics of CO and CO₂ Methanation over nickel,” *Engineering Chemistry Research.*, vol. 60, pp. 5792–5805, 2021.